INFLUENCE OF WELDING PARAMETERS ON THE WELDING RESIDUAL STRESSES

S. GKATZOGIANNIS[*], P. KNOEDEL AND T. UMMENHOFER

KIT Steel & Lightweight Structures
Research Center for Steel, Timber & Masonry
Otto-Ammann-Platz 1, D-76131 Karlsruhe, Germany
e-mail: stefanos.gkatzogiannis@kit.edu, https://stahl.vaka.kit.edu

Key words: FE simulation, welding , AISI 316L, austenitic steel, residual stresses.

Abstract. FE simulation of welds from austenitic steel was carried out in the current paper. Two different multi-pass welds were modelled. Measurements of welding residual stresses, which were found in literature, were applied for the validation of the results. The validated models were then used as basis for sensitivity analysis. The influence of differentiating the welding speed, the heat input of the weld heat source, intermediate cooling between consecutive weld-passes and welding sequence on the welding residual stresses was investigated.

1 INTRODUCTION

Applications regarding finite element (FE) simulation of welds have expanded rapidly in the last decades due to the increased computational power. The significance of the welding residual stresses (WRS) on the fatigue behaviour of metallic components renders their calculation a significant subject of structural engineering. The WRS and mechanical behaviour of the component in general are strongly coupled with the thermal treatment of the component during welding. The thermal history influences the mechanical behaviour due to the temperature dependency of the material parameters of steel and the microstructural transformations that take place inside a thermal cycle, which also influence the final mechanical behaviour.

This coupling is successfully modelled, when welds are simulated by the use of modern FE Multiphysics Software, provided that a robust modelling of all three following fields has been achieved: the thermal, the mechanical and the microstructural behaviour (wherever necessary) of the investigated component during welding. These three fields interact with each other, although the influence of phase changes and mechanical loading on the thermal behaviour and the microstructural behaviour respectively can be neglected with no significant influence on the calculated WRS [1]. The interactions that necessarily have to be modelled in order to ensure robust results are presented in Figure 1.

The use of the double-ellipsoidal model for the heat-source, which was proposed by Goldak in 1984 [2], is considered today state-of-the-art. In combination with the application of modern three-dimensional FE models, due to the increased computational power, it enables precise FE solutions of the heat transfer problem, which show good agreement with measured temperature profiles [1]. Moreover, available data of mechanical behaviour of steel at elevated temperatures is rapidly increasing in the last years. On this basis, the FE models can be used to predict the

temperature distributions during the welding process and their influence on WRS, if the microstructural transformations have also been robustly modelled. Nevertheless, some difficulties arise regarding the applied welding parameters and material models.
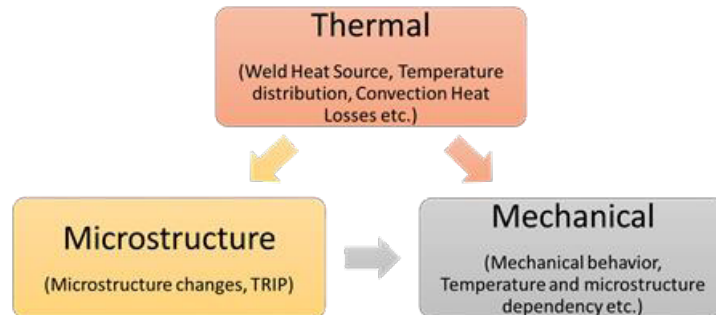

Figure 1: Fields of the weld simulation and interactions taken into consideration

Regarding the welding parameters, the nominal values are usually applied as input during a weld simulation. In practice though, especially in cases where no automated weld-process is applied, welding is carried out under different conditions, especially regarding the welding speed (± 10% deviation is predicted in typical welding procedure specifications (WPS) for the welding parameters). A change of welding parameters, may lead to differentiated WRS profiles. In previous work of the authors for similar components from the same steel grade S355 different WRS profiles were calculated. The resulted longitudinal WRS are presented in Figure 2. Both components were single-pass V grooved welds, with identical weld section geometry and thickness of 5 mm. The first component though, simulated in [1] had length and width of 500 x 200 mm and was supposed to be welded unrestrained with welding speed of 6,7 mm/s (400 cm/min) and effective heat input of 10 kJ/cm. The calculated WRS were compared with profiles from WRS measurements, which were found in [5]. The second one, which is simulated in [4] had length and width of 300 x 300 mm and was restrained during welding. Welding speed and effective heat input in this case were 10 mm/s and 7 kJ/cm respectively. A significant difference between the two calculated profiles is obvious. Reckoning that the boundary conditions have negligible influence on the longitudinal WRS, as it was shown in [6], and the influence of the plate geometry is not expected to cause such a differentiation, as the one presented in Figure 2, the influence of differentiated heat input is obvious. Higher heat input, either through increased heat power of the welding source or lower velocity, is expected to lead to different width of plastic zone and higher strain and stress distributions. Of course, in the case of ferritic or multi-phase steels like S355, the influence of heat input is more complex because it directly effects the cooling behaviour of the component and in extension the microstructure of the fusion zone (FZ) and the heat-affected zone (HAZ). Different microstructure distribution can cause significant differences in the WRS as the mechanical behaviour differs drastically for each steel phase.

On the other hand, uncertainty regarding the applied material parameters, models or applied mechanical restraints is a destabilizing factor in the robustness of results from weld simulations. The temperature dependency of the material parameters, which are applied during a weld modelling, intensifies the influence of heat input. The influence of the temperature-dependent material parameters on the final WRS was studied by Zhu and Chao [8]. Useful simplifications

that retain the preciseness of the results at a required level but also reduce the calculation time or the effort needed for each simulation have been proposed, although a rather primitive 2D model was applied, at least compared to modern 3D possibilities of weld simulation. Teng et al. [7] and Ji et al. [10] applied similar simplified models for investigating the influence of welding sequence in multi-pass butt-welds. In both cases it was successfully proven that selecting appropriate welding sequence during welding, can reduce the tensile WRS confirming textbook knowledge. Nevertheless, reverse welding of selected passes was not investigated.
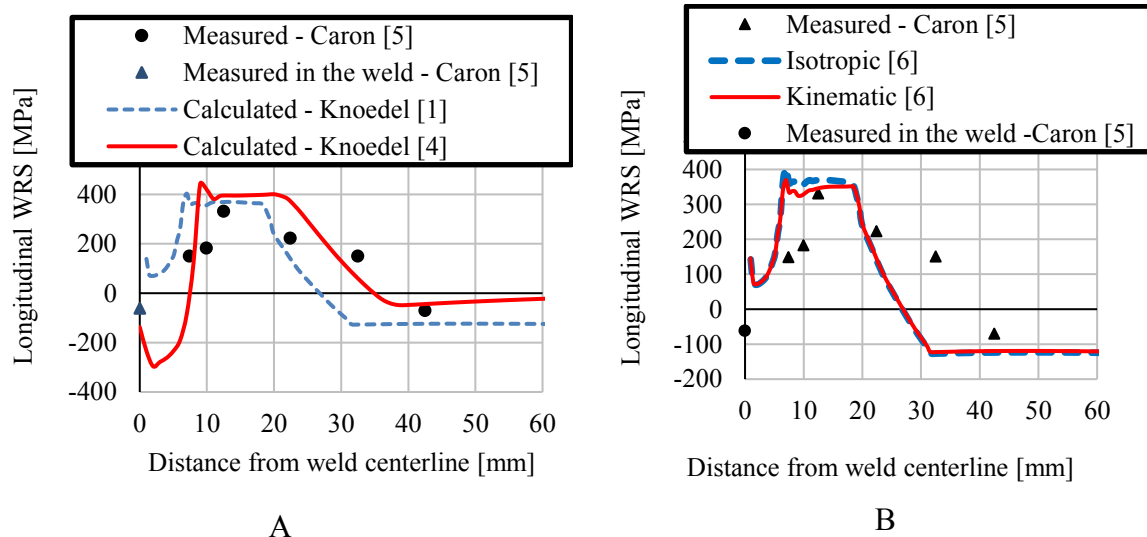

Figure 2: Longitudinal WRS for components from S355 steel – A: Influence of boundary conditions – B: Influence of hardening model

Moreover, more recent studies like those from Gannon et al. [11], Chen et al. [12] and Liu et al. [13] have shown the effectiveness of weld simulation on predicting WRS depending on the welding sequence, by the use of complex modern 3D weld simulation models. These studies focused on the influence of welding sequence on geometries different from a butt-welded plate. The influence of the welding sequence lies on the fact that welding a pass has an effect on the preceding passes, acting for example as thermal stress-relief process. On the other hand, it can result in high cooling rates in the HAZ, producing in this way brittle martensitic microstructures, wherever possible. The effect is therefore more prominent in multi-phase steels. Nevertheless, all the above-mentioned studies investigated austenitic steels, with negligible microstructural changes.

Finally, the influence of the heat input is also significant when the hardening behaviour of steel during reversed plasticity is considered. It was proven in two independent studies from Wohlfart et al. [14] and Mullins and Gunnars [15], that the use of a bilinear isotropic hardening material model during simulation of welding provides WRS with better agreement with measured profiles than kinematic hardening. Both studies were carried out for steels, which in room temperature exhibit the Bauschinger effect and a simulation with a kinematic hardening model would fit better at ambient temperature. It has been proven though by Mataya and Carr [16], that in the case of austenitic stainless steel, when yielding has taken place at elevated temperatures or heat treatment of the material between the consecutive yielding sequences has

taken place, then the Bauschinger effect is eliminated. On the contrary, in a recent study [6] regarding multi-phase single-pass weld from multi-phase S355 steel the kinematic option produced better agreement with measured WRS than the isotropic hardening option (see Figure 3). This could mean that the Bauschinger effect is not temperature-sensitive for carbon steels as in the case of austenitic steels, although the difference between isotropic and kinematic hardening in this case was inside the uncertainty boundaries of weld simulation. More research on this topic is required.

In the current study, a FE model for simulating multi-pass welding of austenitic stainless steel AISI 316L [17] is validated, based on measurements of WRS found in [3]. The model is then applied for a sensitivity analysis in order to define the influence of heat input, deviating from the nominal welding parameters. Moreover, sequence of the welding passes on the calculated WRS of a multi-pass butt-weld is provided. Although numerous papers exist on this subject, they are either applying out-of-date models or investigating different geometries. Finally, applied hardening models and their influence are tested. The phase changes are neglected in all the above cases, which is a standard strategy in the weld simulation of austenitic steels. The investigated material was selected for this reason, so that the influence of the investigated parameters would be directly coupled with the mechanical behaviour of the component, excluding the influence of microstructural changes. The current model will as well act as a stepping-stone, for evolving a model for the simulation of multi-pass welding from multi-phase steel in upcoming studies.

2 THEORETICAL BACKGROUND

During a FE analysis of weld simulation the above mentioned fields, the thermal, the microstructural and the mechanical have to be modelled, so that the WRS can be calculated. Commercial software ANSYS was applied for the present study [17]. The microstructural transformations are neglected in this case and therefore modelling only of the rest two fields is necessary. Temperature dependent material parameters are applied both for thermal and mechanical analyses, ensuring in this way the robust calculation of the WRS.

Modelling of the thermal problem is carried out within a transient thermal analysis. The weld heat source is applied according to the double ellipsoidal model proposed by Goldak [2]. According to Goldak the weld heat source should be modelled as the combination of the halves of two ellipsoids, with same width a and depth b, but different length dimension c. The model is described by the following Equations 1 and 2:

$$q(x,y,z,t) = \frac{6\sqrt{3} f_f Q}{abc\pi\sqrt{\pi}} e^{-3x^2/a^2} e^{-3y^2/b^2} e^{-3[z+v(\tau-t)]^2/c^2} \tag{1}$$

$$q(x,y,z,t) = \frac{6\sqrt{3} f_r Q}{abc\pi\sqrt{\pi}} e^{-3x^2/a^2} e^{-3y^2/b^2} e^{-3[z+v(\tau-t)]^2/c^2} \tag{2}$$

where f_r is the heat fraction deposited in the rear quadrant [J], f_f the heat fraction deposited in the front quadrant [J], Q the energy input rate [J/s], C the characteristic radius of flux distribution [m], v the welding source travel [m/s], t the time [s] and τ a lag factor ("phase shift"). The effective energy input rate is calculated from Equation 5:

$$Q = hVI \tag{3}$$

where V is the voltage around the weld metal arc [V], I the current of the weld metal arc [A] and h the coefficient of the weld heat-source [-]. The heat transfer problem inside the component is governed by the following differential Equation 4:

$$\rho c \left(\frac{\partial T}{\partial t} + v_x \frac{\partial T}{\partial x} + v_y \frac{\partial T}{\partial y} + v_z \frac{\partial T}{\partial z} \right) = \dot{Q}_G + \frac{\partial}{\partial x}\left(Kx \frac{\partial T}{\partial x}\right) + \frac{\partial}{\partial y}\left(Ky \frac{\partial T}{\partial y}\right) + \frac{\partial}{\partial z}\left(Kz \frac{\partial T}{\partial z}\right) \tag{4}$$

where ρ is the density [kg/m^3], c the specific heat [J/(kg K)], T the temperature [K], t the time [s], K_{xx}, K_{yy} and K_{zz} the conductivity in the element's x, y, and z directions respectively [W/(m K)], $\dot{Q}$ the heat generation rate per unit volume [W/m^3] and v_x, v_y, v_z the velocity for transport of heat in x, y, and z directions, respectively [m/s]. Finally the boundary conditions of the thermal transient analysis are the surface heat losses through convection and radiation (Equation 5).

$$\frac{q}{A} = h_f (T_s - T_b) \tag{5}$$

Where q / A is the heat flux out of the face [J/s], h_f the heat transfer coefficient [W/(m^2 K)], T_B the bulk temperature of the adjacent fluid [K] and T_S the temperature at the surface of the model [K]. Ansys' 3D solid element "solid70" is applied for the solution of the transient thermal analysis. A "live and death" procedure is followed, in order to simulate the addition of the filler material and the melting and re-solidifying of the FZ. During this procedure the conductivity of the selected elements, i.e. the elements in the weld pass in front of the moving heat source and all elements with temperature above melting, is reduced by 10^{-6}, while the specific heat and the rest thermal properties are set to zero. At each step of the transient thermal solution the temperature of each node and the sequence of alive and dead elements is saved.

Modelling of the mechanical problem is carried out within a quasi-static structural analysis. Coupling with the thermal analysis is achieved through transfer of the nodal temperature history, which was saved during the transient thermal analysis and application of the transferred temperature as body force nodal loads. Thermal strains are calculated from the temperature history based on Equation 6:

$$\varepsilon^{th} = \alpha^{se}(T)(T - T_{ref}) \tag{6}$$

where $\alpha^{se}(T)$ is the temperature-dependent coefficient of thermal expansion. Ansys' 3D solid elements "solid185" is applied for the solution of the quasi-static structural analysis. The same "live and death" sequence from the transient thermal analysis is being followed also in this part, in order to simulate the influence of the solidifying filler material in the FZ. In this type of analysis, the stiffness of the selected elements in each step is reduced by 10^{-6}, and the strains of the deactivated elements is set to zero. The further steps of the solution are based on classical finite element theory for nonlinear materials.

3   INVESTIGATED CASES

Austenitic stainless steel AISI 316L was investigated in all cases of the current work. Temperature dependent material properties of the investigated material, which were found in [19], are presented in Table 1. Temperature dependent values of the yield strength and tangent modulus of the material were found in [3] (see Figure 3). Two different components were investigated.

Component A consisted of a three-pass V-grooved butt-weld, with dimensions 700 x 700 x 8 mm. The component was identical with the welded component found in [3] and with same mechanical restraints and welding parameters (Table 2), so that a validation with the measured WRS provided by Kyriakongonas et al. [3] was made possible. Calibration of the weld heat source was carried out on a smaller, more efficient component with same weld parameters, weld geometry and plate thickness but with a length and width of 350 mm and 300 mm respectively. Thermocouple measurements on an identical component, which were found in [3], were used for the calibration. Component A was then applied for confirming earlier findings regarding appropriate hardening behaviour (isotropic or kinematic) of austenitic steels.

Component B was a five-pass X-grooved weld with dimensions 300 x 300x 10 mm. The component was assumed to be welded unrestrained and symmetry conditions along the welding line were applied. Similar weld parameters with component A were assumed for modelling component B in the investigated case H1. This case was then used as basis for the sensitivity analysis regarding the differentiated welding speed (investigated cases V1 and V2) and heat input (investigated cases Q1 and Q2), as well the influence of welding sequence (investigated cases R1 - R5) and intermediate cooling between consecutive weld-passes (investigated case C1) on the resulting WRS. The investigated components, their respective welding parameters and all the investigated cases are presented in Figure 4, Table 2 and Table 3 respectively.

4   RESULTS AND DISCUSSION

Modelling of component A was carried out, in order to validate the applied method and the provided material properties. During a successful calibration of the weld heat source through trial and error, appropriate cooling intervals and values for the coefficient of the weld heat source were selected and a satisfying agreement with the thermocouples' measurements provided by [3] was met (see Figure 5). The mechanical behaviour of component A was then modelled based on the provided temperature-dependent material parameters and both isotropic and kinematic hardening behaviours have been applied. The calculated longitudinal WRS along with the respective measured profiles are presented in Figure 5. Against initial expectations and previous findings from other authors ([14] and [15]), the option of the kinematic hardening model produced results that clearly fit better to the measured WRS. Both models produced a WRS profile that fits good with measurements away from the weld region (50mm and further) but only kinematic hardening predicted the WRS in the weld area with preciseness. In both cases the current model seem to be overestimate the width of the tensile stress region and therefore between 10 and 50 mm adjacent to the weld the agreement with measured WRS is not satisfying. Nevertheless, the overall performance was considered adequate. By taking into consideration the even better agreement provided by the FE simulation in [3], with same material models and weld parameters, their application for further investigations on component B was considered valid.

Table 1: Material properties of AISI 316L

Temperature [°C]	Conductivity [W / (m K)]	Specific Heat [kJ / (kg K)]	Density [kg / m³]	Coefficient of Thermal Expansion x 10⁶ [-]	Young's Modulus [GPa]	Poisson's Ratio [-]
20	13,3	0,47	7966	15,2	195	0,267
400	19,4	0,55	7814	17,4	172	0,322
1000	27,5	0,676	7535	19,3	100	0,229
1420	31,9	0,765	7320	20,7	10	0,223
1460	320	0,765	7320	20,7	2	0,223
3000	320	0,765	7320	20,7	2	0,223

During the investigations on Component B, both transverse and longitudinal stresses on both, top and bottom, side of the plate were taken into consideration, as the magnitude of the tensile stresses on each of this cases can have significant influence on the fatigue performance of welded joints. Figure 6 presents the results from investigations on the influence of decreased welding speed or increased heat input.
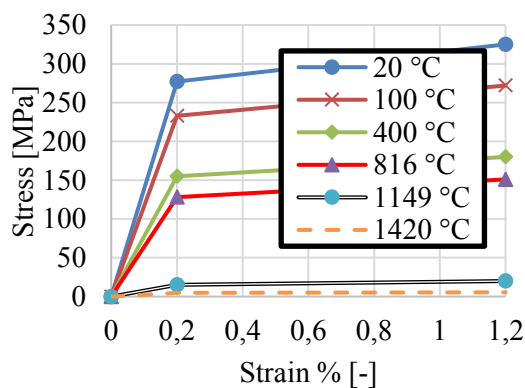

Figure 3: Stress-strain bilinear relationships at different temperature levels for AISI 316L found in [3]

Table 2: Welding parameters for the investigated models

Model	Component A	Component B (investigated case H1)
pass	1-3	1-5
voltage [V]	24	24
current [A]	180	180
welding speed [mm/s - cm/min]	5/30	5/30
welding sequence	A-B-C	A-B-C-D-E
intermediate cooling [s]	800-879-1000	none

The investigated cases are being compared with the investigated case H1. Both the reduction of welding speed and the increase of heat input lead to a beneficial reduction of the longitudinal tensile stresses on the top of the plate, with the reduction of speed at half (V2) producing tensile stresses almost 150 MPa lower than in case H1. The positive effect of the welding speed reduction is obvious also on the transverse WRS profiles on the top of the plate, although it is of a smaller magnitude, around 50 MPa. For cases V1, Q1 and Q2 no significant change is observed in the transverse WRS on the top. On the bottom of the plate (the side of the last weld-pass) all investigated cases provided similar WRS profiles with tensile stresses of the same magnitude and therefore the influence of welding speed and heat input is considered negligible. On the contrary, the application of intermediate cooling between consecutive passes in the investigated case C1 produced WRS profiles with significant increase of tensile stresses in both

longitudinal and transverse directions (see Figure 7). The effect was more profound in the case of transverse WRS on the top of the plate, where an increase of almost 150 MPa was met.
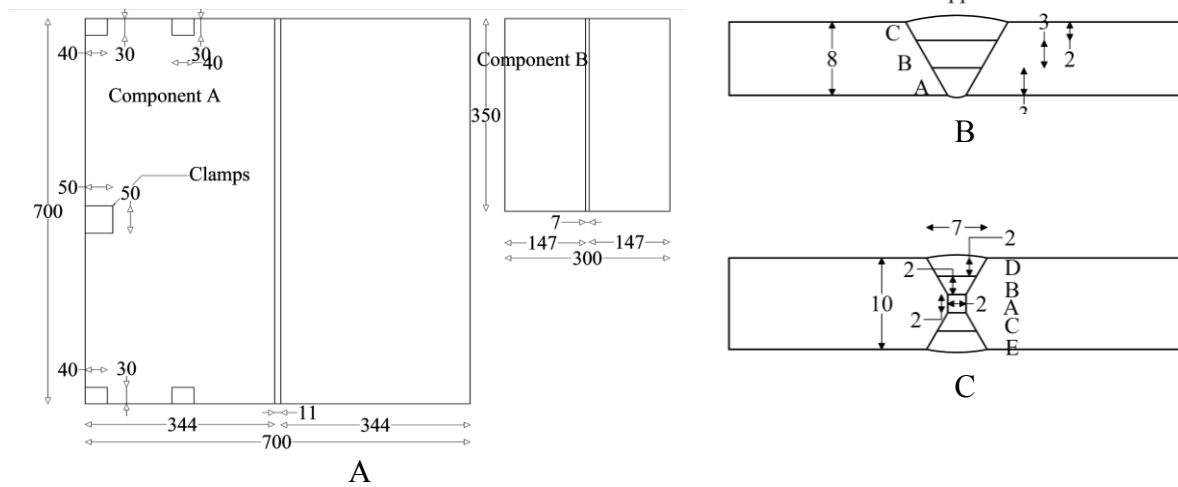

Figure 4: Investigated components – A: Plate dimensions for model A (left) model B (right) B: weld section of component A – C: weld section of component B

Table 3: Investigated cases – Weld passes marked with an apostrophe (B' etc.) are reversely welded

Investigated case	Model	Component	Investigated variable
hardening behaviour	iso	A	isotropic hardening
	kin	A	kinematic hardening
welding parameters	H1	B	welded according Table 2
	V1	B	welding speed – 25% reduced
	V2	B	welding speed – 50% reduced
	Q1	B	heat input - 25% increased
	Q2	B	heat input - 50% increased
	C1	B	intermediate cooling 600s
welding sequence	R1	B	A-B-C-D-E (identical with H1)
	R2	B	A-B'-C-D-E'
	R3	B	A-B-D-C-E
	R4	B	A-B'-D-C'-E
	R5	B	A-B-C-E-D

The results from the investigation of the influence of welding sequence are presented in Figure 8. The current analyses have shown that the anti-symmetric welding sequence A-B-C-E-D, which was modelled in case R5, had a profound effect on the tensile stress in both longitudinal and transverse directions. Maximum calculated tensile stresses on the top of the plate were 450 MPa and 160 MPa in longitudinal and transverse direction respectively, 100 MPa and 30 MPa less than in case R1. Nevertheless, the same sequence produced the highest transverse tensile stresses near the weld area on the bottom of the plate, approximately 25 MPa higher than the rest of the investigated sequences. The influence of this welding sequence on the longitudinal WRS on bottom of the plate is negligible. For the rest of the investigated sequences there was little or no improvement from the symmetric investigated case R1. As a result sequence R5 is considered to be the most advantageous, as the increase of transverse stresses is insignificant,

compared to the decrease of the tensile stresses on top of the plate and the magnitude of the maximum tensile stress is significantly lower than in the rest of the cases.
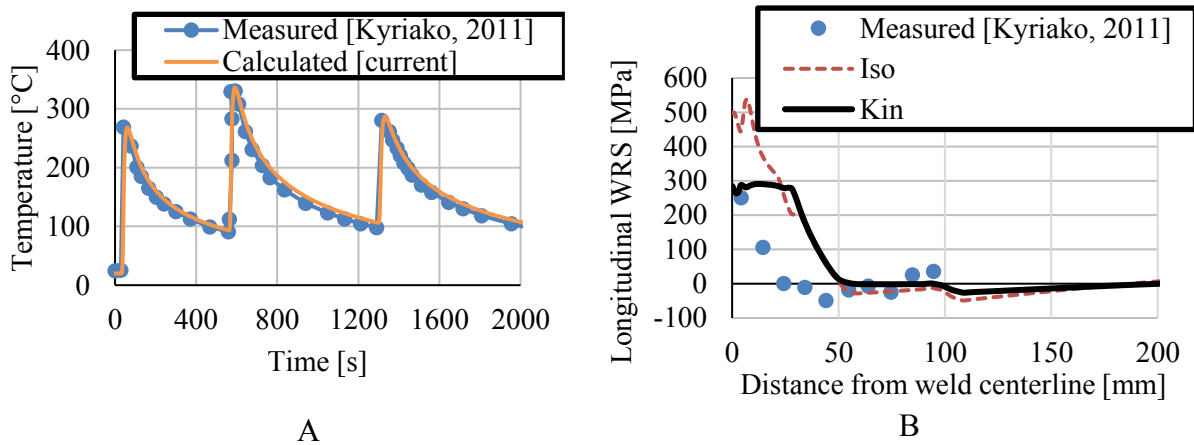

Figure 5: Modelling of component A, measured [3] and calculated profiles – A: Temperature history of node 15 mm adjacent to the weld centreline at the middle on the top of the reduced model – B: Longitudinal WRS on the top of the plate
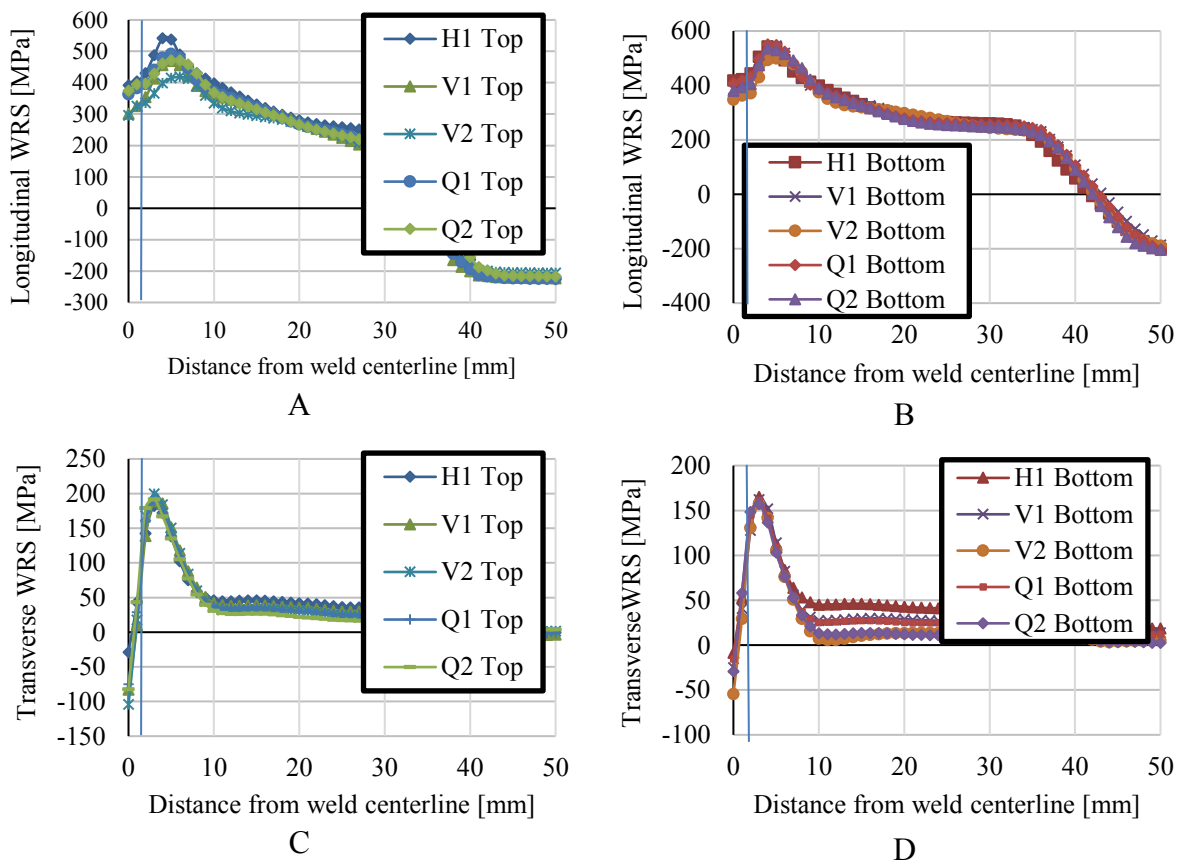

Figure 6: Influence of welding speed and heat input on WRS – A: longitudinal on top of the plate – B: longitudinal on bottom of the plate – C: transverse on top of the plate – D: transverse on bottom of the plate
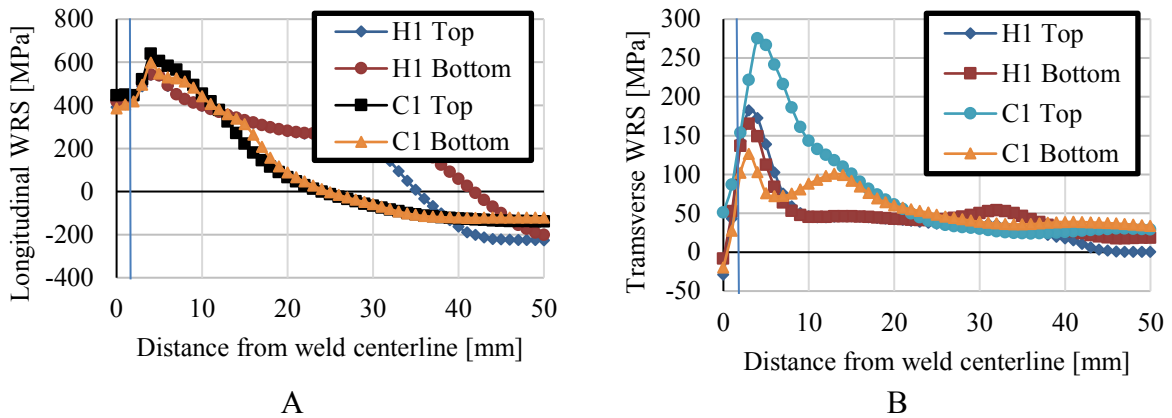
Figure 7: Influence of intermediate cooling – A: on longitudinal WRS – B: on transverse WRS
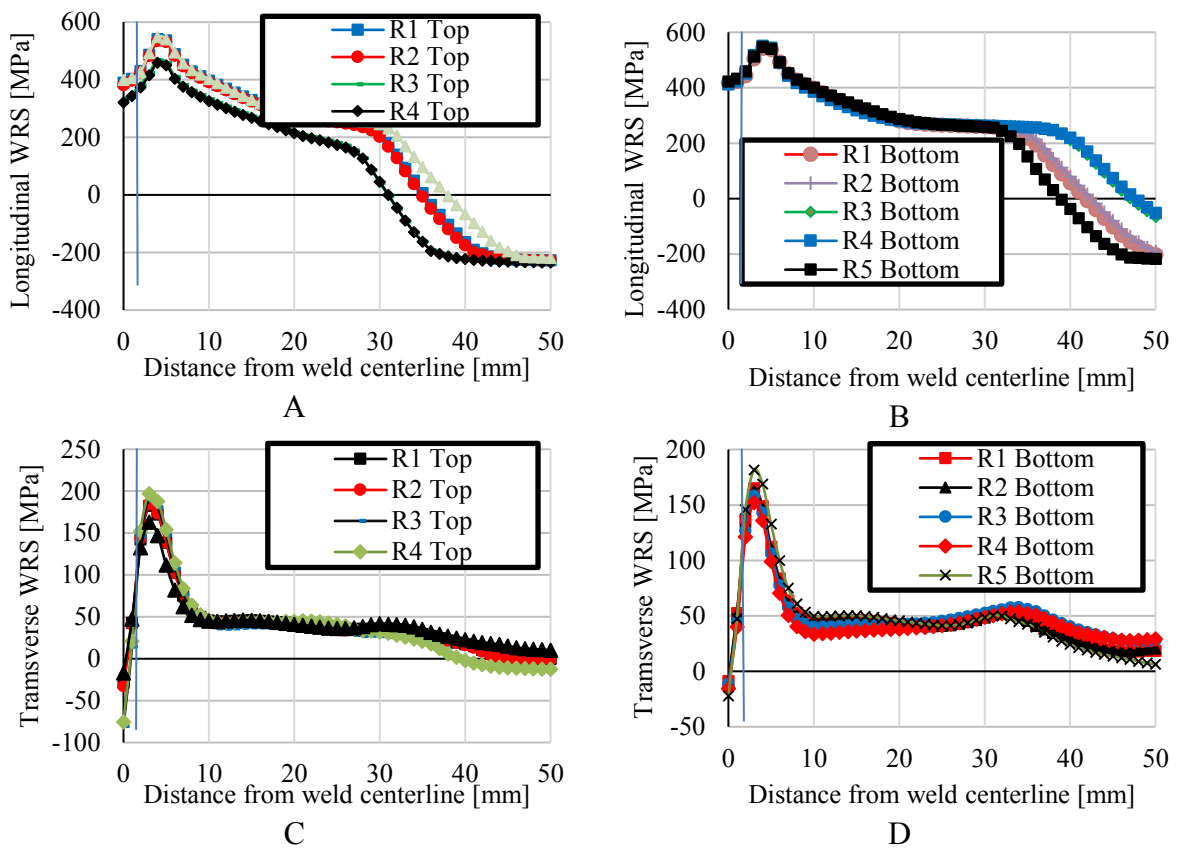

Figure 8: Influence of welding sequence on longitudinal WRS – A: longitudinal on top of the plate – B: longitudinal on bottom of the plate – C: transverse on top of the plate – D: transverse on bottom of the plate

5   CONCLUSIONS AND FUTURE WORK

A series of finite element analyses were carried out in the current paper, so that a sensitivity analysis investigating the influence of various welding parameters could be completed. The applied models were validated based on measurements of WRS found in literature. All the

investigations considered austenitic stainless steel AISI 316L and therefore, no phase transformations were take into consideration. The following safe conclusions could be drawn from the current work:

- Against initial expectations, the option of the kinematic hardening model produced results that clearly fit better to the measured WRS.
- Reduction of welding speed led to reduction of tensile WRS up to 150 MPa and in extension to an optimized predicted fatigue performance of the welded structures. Therefore, reducing welding speed in practice lies on the safe side. Similar, but less profound effect was validated when the heat input of the weld source was increased. Although the heat input rate remains equal in both cases, increase of the heat input and equivalent decrease of welding speed do not produce same WRS profile.
- Intermediate cooling between consecutive weld-passes causes a significant increase of the tensile WRS, even up to 200 MPa. Therefore, it should be avoided in the case of austenitic steels, when the magnitude of tensile stresses is under consideration. On the other hand, prolonged elevated temperatures can cause sigma phase embrittlement. For this reason, it has been "common knowledge" that austenitic steels should be welded as "cold" as possible.
- Antisymmetric welding sequence A-B-C-E-D is proved to be the optimal solution for welding X-grooved 5-pass welds from austenitic steel. A reduction of up to 100 MPa of the longitudinal tensile stresses can be achieved.
- Reverse welding of selected passes seem to have little or no effect on the final WRS, in comparison to the respective forward-only welding sequence.

All the above conclusions can be very useful for the optimization of welding process for austenitic steels. Nevertheless, they cannot be directly adopted for the case multi-phase steels, where microstructural changes can influence profoundly the calculated WRS. The microstructural changes are directly influenced by the investigated variables and further work must be carried out, in order to provide safe conclusions in their case. Finally, reasons for the incompatibility of current and past results regarding the influence of material hardening behaviour on final WRS should be investigated.

ACKNOWLEDGEMENT

REFERENCES

[1] Knoedel, P., Gkatzogiannis, S. and Ummenhofer, T. Practical aspects of welding residual stress simulation. *Journal of Constructional Steel Research* (2017) **132**:83–96.

[2] Goldak, J.A., Chakravarti, A. and Bibby, M. A new finite element model for welding heat sources. *Metall. Trans. B (1984)* **15**:299–305.

[3] Kyriakongonas, A.P., Papazoglou, V.J. and Pantelis, D.I. Complete investigation of austenitic stainless steel multi-pass welding. *Ships and Offshore Structures* (2011) **6**(1–2):127–144.

[4] Knoedel, P., Gkatzogiannis, S. and Ummenhofer T. FE simulation of residual welding stresses: Aluminium and steel structural components. Selected, peer reviewed papers from the 13th International Aluminium Conference INALCO 2016, September 21-23, 2016,

Naples, Italy. *Key Engineering Materials*, (2016) **710**:268-274, Trans Tech Publications, Pfaffikon, Switzerland.

[5] Caron, J., Heinze, C., Schwenk, C., Rethmeier, M., Babu, S.S. and Lippold J. Effect of continuous cooling transformation variations on numerical calculation of welding-induced residual stresses, *Weld. J.* (2010) 89:151-160.

[6] Gkatzogiannis, S., Knoedel, P. and Ummenhofer, T. FE welding residual stress simulation. Influence of boundary conditions and material models. EUROSTEEL 2017, September 13–15, 2017, Copenhagen, Denmark, (2017), full paper submitted.

[7] Teng, T.L., Chang, P.H. and Tseng, W.C. Effect of welding sequences on residual stresses. *Computers and Structures* (2003) **81**:273–286.

[8] Zhu, X.K. and Chao, Y.J. Effects of temperature-dependent material properties on welding simulation. *Computers and Structures* (2002) **80**:967–976.

[9] Teng, T.L. and Chang, P.H., Tseng, W.C. Effect of welding sequences on residual stresses. *Computers and Structures* (2003) **81**:273–286.

[10] Ji, S.D., Fang, H.Y., Liu, X.S. and Meng, Q.G. Influence of a welding sequence on the welding residual stress of a thick plate. *Modelling Simul. Mater. Sci. Eng.* (2005) **13**:553–565.

[11] Gannon, L., Liu, Y., Pegg, N. and Smith, M. Effect of welding sequence on residual stress and distortion in flat-bar stiffened plates. *Marine Structures* (2010) **23**:385–404.

[12] Chen, Z., Chen, Z. and Shenoi, R.A. Influence of welding sequence on welding deformation and residual stress of a stiffened plate structure. *Ocean Engineering* (2015) **106**:271-280.

[13] Liu, C., Luo, Y., Yang, M. and Fu, Q. Three-dimensional finite element simulation of welding residual stress in RPV with two J-groove welds. *Weld World* (2017) 61:151–160.

[14] Wohlfahrt, H., Nitschke-Pagel, T., Dilger, K., Siegele, D., Brand, M., Sakkiettibutra, J. and Loose, T. Residual stress calculations and measurements – Review and assessment of the IIW round robin results. R*ecommended for publication by commission X: Structural Performances of Welded Joints – Fracture Avoidance*. (2012) Doc. IIW **2224**:120-140.

[15] Mullins, J. and Gunnars J. Influence of hardening model on weld residual stress distribution. Research Report 2009:16, Inspecta Technology AB, Stockholm, Sweden, (2009).

[16] Mataya, M.C. and Carr, M.J. The Bauschinger effect in a nitrogen-strengthened austenitic stainless steel. *Materials Science and Engineering* (1983) **57**:205-222.

[17] ASTM A240/A240M-16a Standard Specification for Chromium and Chromium-Nickel Stainless Steel Plate, Sheet and Strip for Pressure Vessels and for General Applications, ASTM International, West Conshohocken, PA, 2016

[18] ANSYS® Academic Research, Release 17.2, Help System, ANSYS, Inc., (2016).

[19] Dong, P. Residual stress analyses of a multi-pass girth weld: 3-D special shell versus axisymmetric models. *Journal of Pressure Vessel Technology* (2001) **123**:207-213.

[20] Gkatzogiannis, S. PhD Thesis (in progress), KIT, Karlsruhe Institute of Technology, Steel and Lightweight Structures, 2017.